Molecular Catalysis 453 (2018) 100–112

Contents lists available at ScienceDirect

Molecular Catalysis

journal homepage: www.elsevier.com/locate/mcat

Full length article

The catalytic CO oxidative coupling to dimethyl oxalate on Pd clusters anchored on defected graphene: A theoretical study

Lixia Ling[a,b], Xue Feng[a], Yueting Cao[a], Ping Liu[b], Maohong Fan[c], Riguang Zhang[d], Baojun Wang[d,*]

[a] College of Chemistry and Chemical Engineering, Taiyuan University of Technology, Taiyuan, 030024, PR China
[b] State Key Laboratory of Coal Conversion, Institute of Coal Chemistry, Chinese Academy of Sciences, Taiyuan, 030001, PR China
[c] Department of Chemical and Petroleum Engineering, University of Wyoming, 1000 E University Ave, Laramie, WY, 82071, USA
[d] Key Laboratory of Coal Science and Technology of Ministry of Education and Shanxi Province, Taiyuan University of Technology, Taiyuan, 030024, PR China

ARTICLE INFO

Keywords:
CO oxidative coupling
Pd clusters
Defected graphene
Activity and selectivity
Dimethyl oxalate

ABSTRACT

The catalytic CO oxidative coupling to dimethyl oxalate (DMO) was studied by means of density functional theory (DFT) calculations, and effects of different sizes of Pd_n cluster and different defective graphenes on this reaction were also discussed. A series of different sizes of Pd_n (n = 1, 4 and 6) anchored on single-vacancy graphene (SVG) was firstly constructed, and the results show that the Pd-SVG catalyst shows remarkable catalytic activity for CO oxidative coupling to DMO. In addition, the single Pd atom supported on different defective graphenes were studied to reveal the effect of the vacancy type of graphene on reaction activity and selectivity. It showes that the favorable pathway is CO−$COOCH_3$ coupling path on the Pd supported on the graphene with double vacancy (DVG), which has excellent activity and selectivity. Therefore, Pd-DVG can be considered as effective catalyst to enhance the catalytic performance and greatly reduce cost of noble Pd-based catalysts.

1. Introduction

Dimethyl oxalate (DMO) is an important raw chemical material in industry, which is commonly used as solvent, extraction agent, and also serves as feedstock for the syntheses of oxalic acid, oxamide, dyes, pharmaceuticals, *etc* [1,2]. More importantly, DMO hydrogenation is the main source of ethylene glycol (EG) [3–6]. CO oxidative coupling will lead to the formation of DMO, which is considered to be one of the most important applications in C1 chemistry [7]. Pd-based catalysts have been proved to possess high activity and selectivity for the CO oxidative coupling to DMO *via* lots of experimental and theoretical studies [8–12]. However, this technology is limited in industrial applications on a large scale due to the shortage of Pd resources and the high price of noble metal Pd [13]. Aiming at this situation, it is an urgent problem to find an excellent catalyst with a small amount of Pd, but with high catalytic activity and selectivity for CO oxidative coupling to DMO.

Noble metals clusters with a few atoms can largely reduce the loading amount of noble metals, and show unique chemical and physical properties [14,15], which have received widespread attention and application, such as the treatment of automobile exhaust gas [16,17], selective catalytic reduction reaction [18,19], as well as CO oxidative reaction [20–22]. The catalytic activity of Pd_n clusters is influenced greatly by the quantum size, and which can be improved by adjusting the size dimension. Adsorptions of CO and NO, as well as the CO + NO reaction on Pd_n clusters [18,19] have been studied, it shows that clusters with different sizes show different reaction mechanisms. Xiao et al. [23] have investigated hydrogen adsorption on Pd_n (n = 1–5) clusters which are supported on graphene by systematic density-functional theory and showed that the hydrogen adsorption on the Pd_n (n ≥ 3) clusters is stronger than on Pd(111). Previous report has been revealed that Pd_6 clusters doped single defective graphene is more advantageous as adsorbent material for AsH_3 removal compared with Pd supported on single defective graphene and Pd_4 supported on single defective graphene [24]. Recently, single-atom catalysts has shown an excellent catalytic activity and selectivity with minimal noble metal usage and high atom efficiency. Thus it has been investigated as a promising type of catalyst for various reactions [25,26]. The single-atom Pd-VG catalyst showed excellent selectivity and durability against deactivation during the selective hydrogenation of 1, 3-Butadiene for a total 100 h [27]. Experimental results exhibited that Pt-FeO_x is 2–3 times more active than the sub nanometer-sized catalysts for CO oxidation, and is stable during a long term test [28]. Hackett et al. [29] showed that atomically dispersed Pd^{II} on Al_2O_3 was much more active

* Corresponding author.
E-mail addresses: wangbaojun@tyut.edu.cn, wbj@tyut.edu.cn (B. Wang).

https://doi.org/10.1016/j.mcat.2018.04.021
Received 8 March 2018; Received in revised form 19 April 2018; Accepted 19 April 2018

for the selective aerobic oxidation of allylic alcohols than Pd clusters and nano-particles on the same support.

Single-atom catalysts can maximize the efficiency of metal utilization due to well-defined and uniform single-atom dispersion on supports [30], and different types of supports have been studied, including metal oxides [31–33], metal surfaces [34], and graphene *etc* [35–37]. Among them, graphene received widespread attention because of unique properties, such as large surface area, high carrier mobility, good mechanical properties, high thermal conductivity, and so on [38,39]. Defects on graphene can facilitate the interaction between the metal atom and graphene sheet for graphene-based single-atom catalysts [40]. Up to now, intrinsic point defects on graphene, including vacancies, topological defects and adatoms, have been experimentally observed, and which influence physical and chemical characteristics of graphene [41–47]. Single-vacancy and double-vacancy are typical and common defects produced by missing the lattice atom [48–51]. The stability and electronic structures of Pd_n (n = 1–5) clusters supported on single-vacancy graphene surface have been studied, it showed that point defect acts as a strong binding trap for Pd clusters and is favorable for the dispersion of the Pd nanoparticles [52]. Similar results are also found that oxygen molecule preferred to be chemisorbed on the graphene surface containing vacancy-defect sites compared to the perfect surface by Qi et al. [53] In addition, the electronic ground state of the double vacancy defect possesses 70% closed shell character which indicates a significantly chemical stability as compared to the single-vacancy case has been shown by Machado et al. [54] Besides intrinsic point defects, a suitable dopant is considered to be a significant and effective way to improve the chemical activity and electric properties of carbon nanomaterials. Non-metal atoms (B, N, S) can effectively alter the properties of graphene [55–57]. B-doped and N-doped carbon materials have been synthesized [58] by an arc-discharge method and studied extensively [59–61]. N-doped graphene materials as catalysts for oxygen reduction reaction (ORR) were tested and showed better catalytic activity than that of pure graphene and commercial XC-72 due to N incorporation [62]. Moreover, N-doped graphene can exhibit an n-type behavior and lead to a decreased conductivity, an improved on/off ratio and a Schottky barrier with the electrodes by electrical measurements [63]. Simultaneously, boron as heteroatom has also been introduced in graphene to modify electronic and physicochemical properties. The B-doped graphene can serve as an efficient metal-free catalyst for hydrogen evolution reaction compared to defective graphene [64]. Thus, atomic doped graphene with the type of defects in also plays an important role in the reaction activity.

In this work, Pd clusters with different sizes supported on the single-vacancy graphene are investigated to find the appropriate Pd metal size, and then which is supported on graphene with different defects to reveal the effect of the defective type of graphene on reaction activity. Finally, an optimal catalyst with a little amount of Pd and high activity will be obtained, and the selectivity will also be investigated.

2. Calculation details

2.1. Method

The DMol^3 program package in Material Studio 5.5 was designated to perform all density functional calculations [24,65]. The generalized gradient approximation (GGA) with Perdew-Burke-Ernzerhof (PBE) functional [66,67] was selected to calculate the exchange and correlation energies. The doubled-numerical quality basis set with polarization functions (DNP) [68,69] was employed with the effective core potentials (ECP) scheme [70,71]. The real space cutoff radius was 4.8 Å. The integration of the Brillouin zone was calculated using 3 × 3 × 1 *k*-point sampling for 6 × 6 pristine graphene (PG) super-cells in a periodic system (total of 72 carbon atoms) according to previous results [72–74]. The thermal smearing level was set at 0.005 Ha (1 Ha = 2625.5 kJ mol^{-1}) to achieve accurate electronic convergence. And no symmetry and spin polarization were allowed [75]. For geometrical optimizations, the total energy, the maximum force and the maximum displacement were converged to 2×10^{-5} Ha, 4×10^{-3} Ha/Å and 0.005 Å, respectively. Plane-wave electronic density functional theory with long range dispersion interaction corrections DFT-D was considered to balance computational efficiency and accuracy.

The complete LST/QST method was selected to search the transition states (TS) for every elemental step during the CO oxidative coupling to oxalate [76,77]. In the meantime, TS confirmation was carried out to confirm the accuracy of the transition state.

The binding energy (E_b) has been considered for the structural stability of Pd_n/graphene (n = 1, 4, 6), E_b was calculated according to Eq. (1):

$$E_b = (E_{Pdn} + E_{graphene} - E_{Pdn/graphene}) \quad (1)$$

where $E_{Pdn/graphene}$, E_{Pdn} and $E_{graphene}$ were total energies of Pd_n, graphene and Pd_n/graphene (n = 1, 4, 6), respectively.

The activation energy of elementary step was calculated according to the following equation:

$$E_a = E_{TS} - E_R \quad (2)$$

where E_{TS} and E_R were total energies of the transition state and the reactant. A smaller value of the activation energy means a more favorable kinetic process.

2.2. Model

In this study, pristine graphene was firstly optimized, and the lattice parameter is a = b = 2.466 Å, which was in good agreement with experimental results [78,79] and our previous result [80]. A $p(6 \times 6)$ supercell was chosen, which was enough to avoid interaction between periodic images along the surface. The vacuum region in the model structures was set to 15 Å in order to avoid interactions between two successive layers along *z*-axis, and C atoms at the edge were fixed to ensure that the interaction between periodic vacancy defects was negligible. Then, single-vacancy and double vacancy as two typical vacancy defects were considered [81,82]. The single-vacancy defective graphene (SVG) was constructed by removing one C-atom from the perfect graphene and leaving each of three neighboring C-atoms with sp^2 dangling bonds. The double-vacancy defective graphene (DVG) was built by removing two neighboring C-atom from the perfect graphene, which is comprised of two pentagonal rings and one octagonal ring referred to as the 5-8-5 defect [55]. It has high stability and a symmetry of the defect ring [83]. Moreover, the doped structures were modeled by replacing one of the carbon atoms in the single-vacancy defective region by the other selected heteroatom (N or B) [76,84], namely, N-doped single-vacancy graphene (NVG) or B-doped single-vacancy graphene (BVG). The optimized structures of different vacancy graphene were also shown in Fig. 1.

3. Results and discussion

3.1. Stability of Pd_n-SVG (n = 1, 4, 6), Pd-DVG, Pd-NVG and Pd-BVG

The isolated Pd atom has a strong affinity to the C defected site on the SVG with a high binding energy of 545.8 kJ mol^{-1}, and consistent with the previous work [24,70,81]. The nearest Pd–C bond length is 1.959 Å in Pd-SVG [84], and the height of Pd atom above the graphene sheet is 1.732 Å due to the larger radius of Pd than that of C atom, see Fig. 2 and Table 1. For small Pd_n (n = 1–7) clusters, Pd_4 and Pd_6 clusters are magic number clusters, possess the special stability by the analysis of second energy difference Δ_2E in previous study [85,86]. The stable Pd_4 cluster is tetrahedral and the octahedron Pd_6 is the most stable configuration [53,87]. Three different interaction modes between Pd_n and SVG are considered through top Pd atom, the Pd-Pd bridge and the Pd-Pd-Pd surface with the single-vacancy site [78]. The

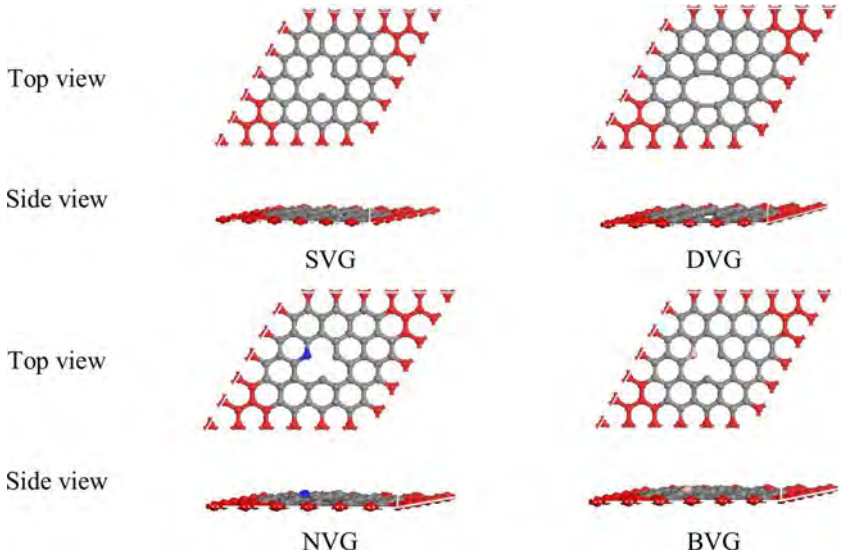

Fig. 1. The optimized slab models of SVG, DVG, NVG, BVG surface. The red and dark grey spheres represent the fixed and relaxation carbon atoms, respectively. (For interpretation of the references to colour in this figure legend, the reader is referred to the web version of this article.)

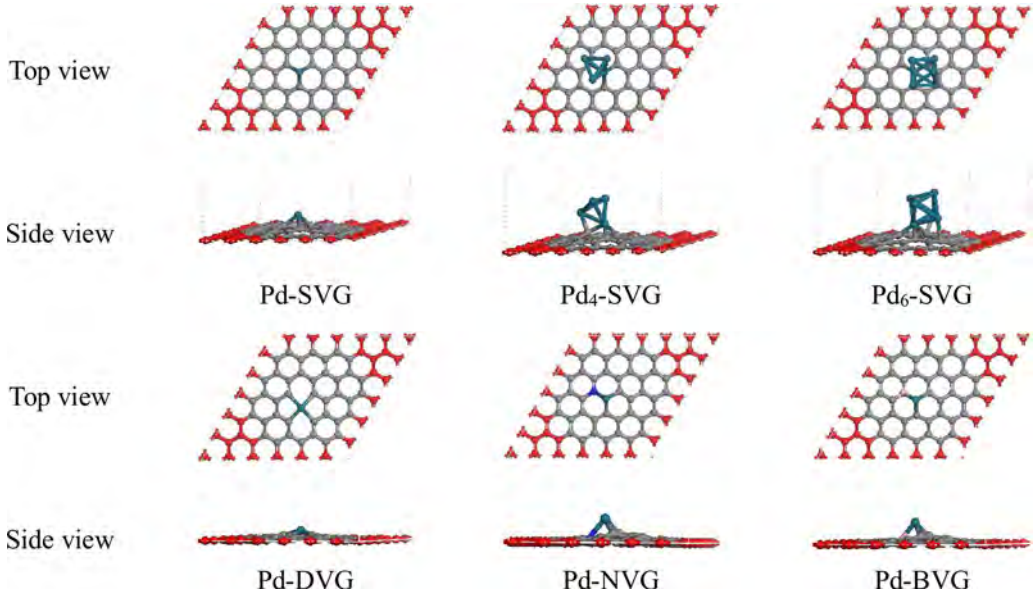

Fig. 2. The most stable configurations of Pd_n(n = 1, 4, 6) clusters on the SVG surface, as well as the most stable configurations of Pd-DVG, Pd-NVG and Pd-BVG.

Table 1
Energetic and structural properties for different defective graphenes supported Pd atom. The properties listed are the smallest Pd-C distance ($d_{Pd\text{-}C}$), the smallest Pd-X distance ($d_{Pd\text{-}X}$), the average Pd-Pd distance ($d_{Pd\text{-}Pd}$), Pd atom height (h), and the binding energy (E_b).

Parameters	Pd_6-SVG	Pd_4-SVG	Pd-SVG	Pd-DVG	Pd-NVG	Pd-BVG
$d_{Pd\text{-}C}$ (Å)	1.944	1.956	1.959	2.017	1.954	1.966
$d_{Pd\text{-}X}$ (Å)	–	–	–	–	2.238	1.999
$d_{Pd\text{-}Pd}$ (Å)	2.692	2.650	–	–	–	–
h (Å)	1.904	1.901	1.732	0.880	1.798	1.849
E_b (kJ mol^{-1})	681.6	615.2	545.8	485.6	366.4	454.9

most stable Pd_4-SVG is obtained when Pd_4 interacts with graphene *via* the Pd-Pd bridge and the C-vacancy of graphene with the E_b of 615.2 kJ mol^{-1}, which has also been shown by Jia et al. [53] The average Pd-Pd bond length of Pd_4 on SVG (2.650 Å) slightly elongated compared with the gas-phase bond length of 2.564 Å, indicating that there is a little effect of SVG on Pd clusters. A similar situation occurs in Pd_6-SVG, the most stable configuration is octahedral double triangular pyramid with one Pd atom bounds to carbon vacancy site and other two Pd atoms also bound to the substrate. Pd_6-SDG has the strongest binding energy of 681.6 kJ mol^{-1} compared with Pd atom and Pd_4 deposition on the single-vacancy defective graphene, which was verified by previous studies [53]. The average Pd-Pd bond length of Pd_6-SVG has a slight enhancement (2.962 Å) compared with Pd_4-SVG. It can also be seen that the binding energies of single-vacancy defective graphene supported Pd_n (n = 1, 4 and 6) clusters increase monotonously with the increase of cluster size.

At the same time, we also constructed three different configurations (Pd-DVG, Pd-NVG and Pd-BVG) in order to explore effects of different defects and heteroatoms of graphene surfaces on reaction activity. The most stable configurations of Pd-DVG, Pd-NVG and Pd-BVG are shown in Fig. 2. It can be seen that Pd atom bounds on vacancy sites, respectively. Pd atom protrudes from the vacancy defective graphene surface due to the larger atomic radius of Pd atom. Pd-DVG has a smaller height between Pd atom and the graphene sheet with 0.880 Å

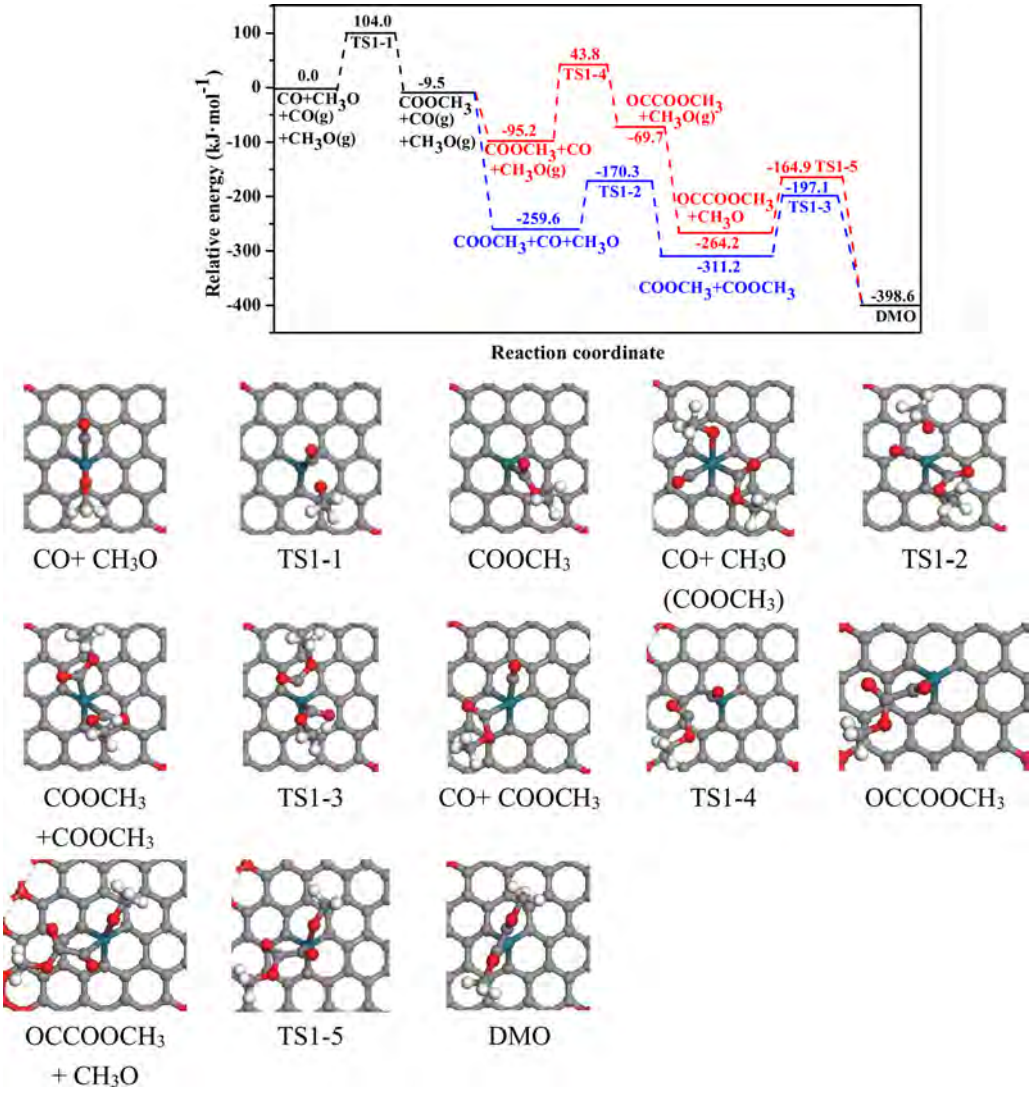

Fig. 3. Potential energy diagram of correlation reactions of CO oxidative coupling to DMO, and configurations of initial states, transition states and final states on Pd-SVG.

than that in other models, this is due to the double vacancy can form a larger space for Pd atom deposition. As a result, the hybridization between B (N) and C atoms around the vacancy decreases the binding energy.

3.2. Activities of single-vacancy graphene supporting Pd_n (n = 1, 4, 6) clusters

CO oxidative coupling to DMO is the crucial step in the realization of the conversion of C1 to C2 in CTEG, and is one of the important topics in the research of C1 chemistry [88,89]. CO oxidative coupling reaction starts with CO and CH_3O because CH_3ONO can easily dissociate into the CH_3O and NO on the Pd-based catalysts [90,91]. Meanwhile, NO is recycled to regenerate CH_3ONO, which is a rapid reaction at ambient temperature without any catalyst [92]. Hence, the effect of NO on the reaction will not be discussed in following sections.

Three possible pathways were proposed in previous studies [3], including $COOCH_3$—$COOCH_3$ coupling path, CO—$COOCH_3$ coupling path and CO—CO coupling path. However, CO—CO coupling will not be considered, since OCCO intermediate cannot be stably existed in this catalytic reaction system. Therefore, two possible pathways for CO oxidative coupling to DMO have been considered in this work, namely $COOCH_3$—$COOCH_3$ coupling route (Path 1) and CO—$COOCH_3$ coupling route (Path 2).

$$\text{Path 1: } CO + CH_3O \rightarrow COOCH_3 \xrightarrow{+CO+CH_3O} COOCH_3 \xrightarrow{COOCH_3} DMO$$

$$\text{Path 2: } CO + CH_3O \rightarrow COOCH_3 \xrightarrow{+CO} OCCOOCH_3 \xrightarrow{+CH_3O} DMO$$

3.2.1. CO oxidative coupling to DMO on Pd-SVG

CO oxidative coupling reaction is initiated by co-adsorption of CO and CH_3O on Pd-SVG surface, in which CO and CH_3O are obliquely adsorbed on Pd atom. It is indicated that the noble metal Pd is the active site for the reaction. Single metal atom is as the active site but not support has been proved in previous studies [93]. CO is stably adsorbed on the Pt atom in Pt-SVG [94], and Au single atom can be extremely active for CO oxidation when Au is dispersed on suitable oxide supports. Then, CH_3O oxidizes CO to form the common intermediate $COOCH_3$ *via* TS1-1, an energy barrier of 104.0 kJ mol^{-1} is needed, as shown in Fig. 3. In Path 1, the other $COOCH_3$ is formed between CO and CH_3O *via* TS1-2 with an energy barrier of 89.3 kJ mol^{-1}. And then, two $COOCH_3$ molecules can stably exist on single-atom Pd due to large co-adsorption energy of −382.0 kJ mol^{-1}, and coupled with each other to form DMO *via* a new C—C bond with an energy barrier of 114.1 kJ mol^{-1}, this is the rate-limiting step for Path 1. In Path 2, the formation of intermediate $OCCOOCH_3$ by CO

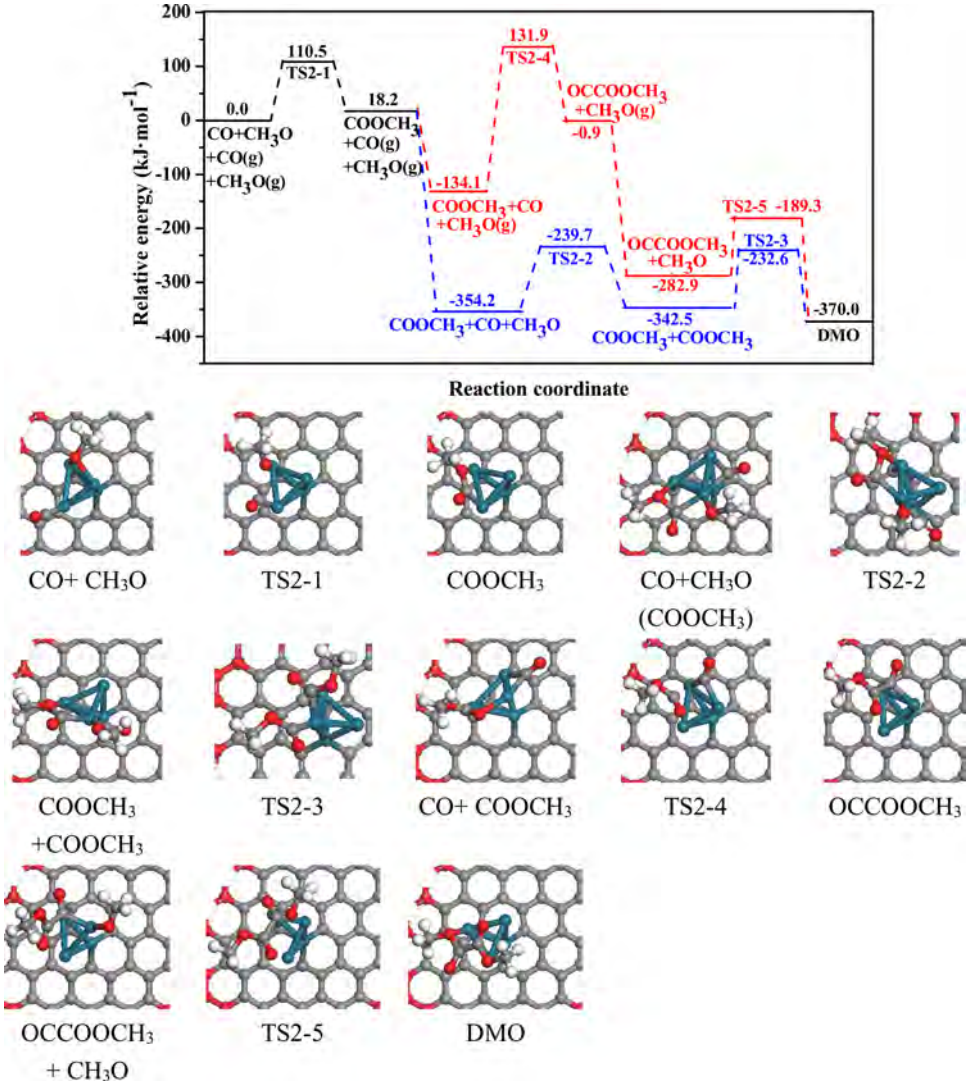

Fig. 4. Potential energy diagram of the correlation reaction of CO oxidative coupling to DMO and the configuration of initial states, transition states and final states on Pd_4-SVG.

connecting with $COOCH_3$, which is the rate-limiting step with a higher activation energy of 139.0 kJ mol^{-1} and form a new C—C bond. Finally, CH_3O attacks $OCCOOCH_3$ to generate DMO *via* TS1-5, this elementary reaction needs to overcome an energy barrier of 99.3 kJ mol^{-1}. We can see that the rate-limiting steps of these two pathways are $COOCH_3 + COOCH_3 \rightarrow$ DMO and $CO + COOCH_3 \rightarrow OCCOOCH_3$ with the corresponding activation energy of 114.1 and 139.0 kJ mol^{-1}, respectively. As a result, the most favorable pathway of CO oxidative coupling to DMO is $COOCH_3$—$COOCH_3$ coupling route, but the CO—CO coupling route is the advantageous route on the Pd(111) surface [3]. In addition, they are with similar energy barriers of the rate-limiting step on Pd-SVG and Pd(111) surface (114.1 and 114.6 kJ mol^{-1}).

3.2.2. The catalytic reaction of CO on Pd_4-SVG

We considered all possible reaction pathways for each elementary reaction in CO oxidative coupling to DMO on Pd_n (n = 4 and 6) supported on single-vacancy graphene catalysts, including reactive species on different adsorption sites. The potential energy diagram of the favorable reaction path on Pd_4-SVG catalyst is shown in Fig. 4. For the first step, $CH_3O + CO \rightarrow COOCH_3$, in the reactant, CH_3O adsorbs at bridge site and attacks CO at an adjacent top site, it needs to overcome an energy barrier of 110.5 kJ mol^{-1} to form $COOCH_3$. Subsequently, the second of $COOCH_3$ is produced *via* TS2-2, which overcomes an energy barrier of 114.5 kJ mol^{-1}. This elementary reaction is the rate-limiting step in Path 1. Then the C—C coupling reaction carries out between two $COOCH_3$ with an energy barrier of 109.9 kJ mol^{-1} to form produce DMO. For CO—$COOCH_3$ coupling in Path 2, $COOCH_3$ reacts with CO *via* TS2-4 to form a stable intermediate $OCCOOCH_3$, it needs to overcome a high energy barrier of 266.0 kJ mol^{-1}, and it is the speed control step. Finally, CH_3O attacks $OCCOOCH_3$ *via* TS2-5 to form DMO, the energy barrier and reaction energy are 93.5 and −87.1 kJ mol^{-1}. As mentioned above, the rate-determining steps of Path 1 and Path 2 on Pd_4-SVG catalyst is $CO + CH_3O$ $(COOCH_3) \rightarrow COOCH_3 + COOCH_3$ and $CO + COOCH_3 \rightarrow OCCOOCH_3$ with the energy barriers of 114.5 and 266.0 kJ mol^{-1}, respectively. It shows that Path 1 is more advantageous than Path 2. In addition, Pd_4 cluster supported on SVG exhibits similar catalytic activity than single-atom Pd (114.5 *vs* 114.1 kJ mol^{-1}).

3.2.3. The formation of DMO on Pd_6-SVG

The reaction path is the same as that on Pd-SVG and Pd_4-SVG catalysts, as shown in Fig. 5. The co-adsorption of CO and CH_3O on Pd_6-SVG with CH_3O at a bridge site and the CO vertically at the adjacent top site is as the reactant. Then CH_3O attacks CO to form $COOCH_3$ *via* TS3-1, which needs to overcome a little energy barrier of 72.3 kJ mol^{-1}. Subsequently, two different possible pathways will be gone. The second $COOCH_3$ is formed *via* CH_3O and CO with TS3-2, which must surmount

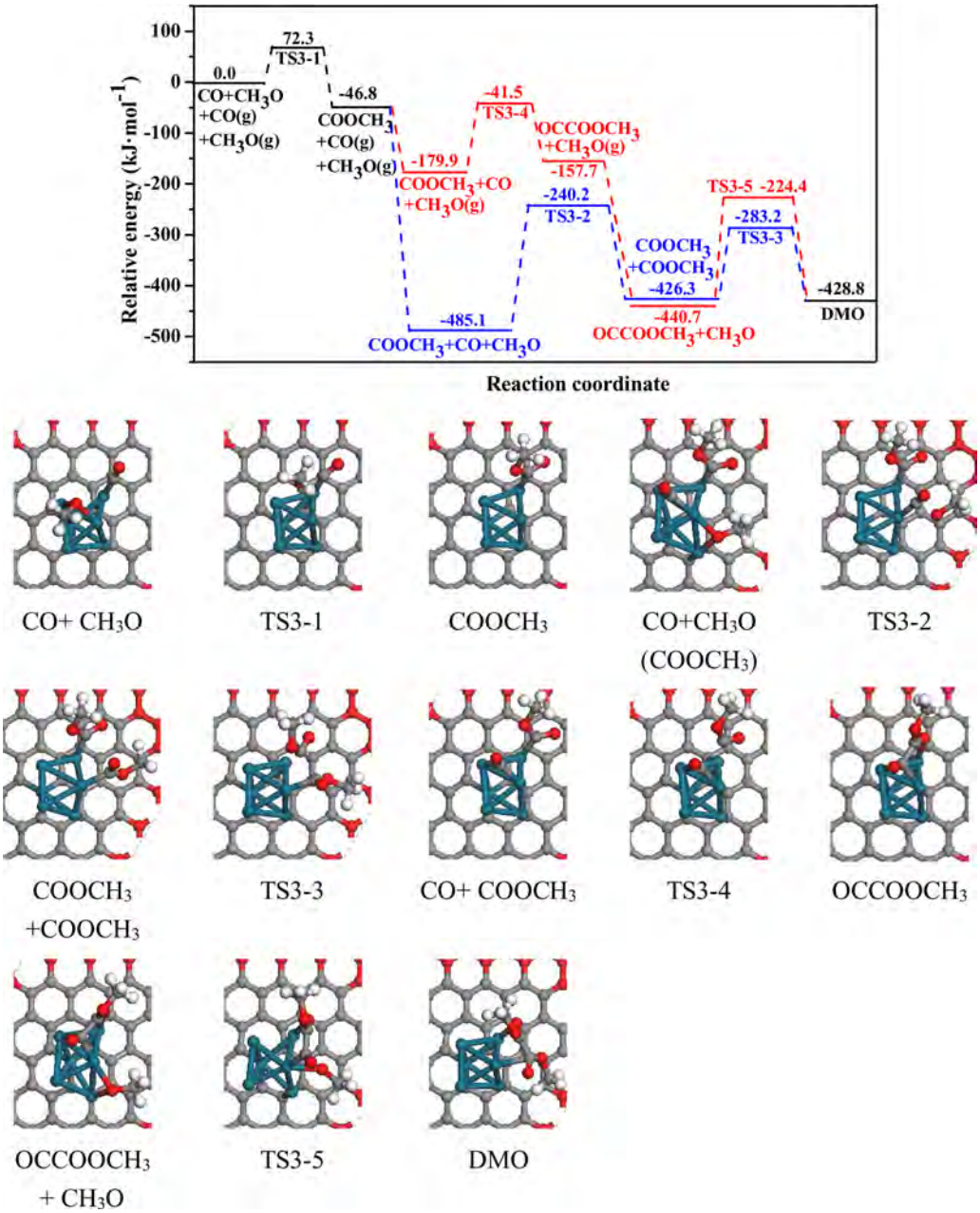

Fig. 5. Potential energy diagram of the correlation reaction of CO oxidative coupling to DMO and the configuration of initial states, transition states and final states on Pd_6-SVG.

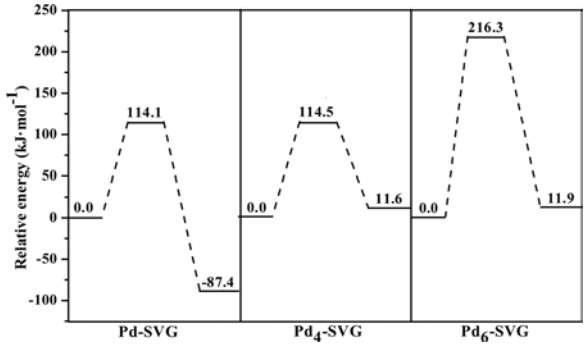

Fig. 6. The comparison of the simplified potential energy profile for the most favorable formation pathway of CO oxidative coupling to DMO on Pd-SVG, Pd_4-SVG and Pd_6-SVG.

a high energy barrier of 244.9 kJ mol^{-1} in the $COOCH_3$—$COOCH_3$ coupling route. In the last step, DMO is formed followed by two $COOCH_3$ coupling with each other *via* TS3-3, which has an energy barrier and an exothermic energy of 143.1 and 2.5 kJ mol^{-1}, respectively. For Path 2, C—C coupling between $COOCH_3$ and CO to form $OCCOOCH_3$ *via* TS3-4, this process is accompanied by endothermic heat of 22.2 kJ mol^{-1} with an energy barrier of 138.4 kJ mol^{-1}. Finally DMO is formed by CH_3O attacking $OCCOOCH_3$ *via* TS3-5, which needs to overcome an energy barrier of 216.3 kJ mol^{-1} with an endothermic energy of 11.9 kJ mol^{-1}.

To summarize, CO—$COOCH_3$ coupling route is the favorable path for the formation of DMO, and $OCCOOCH_3$ + CH_3O → DMO is the rate-determining step with the energy barrier of 216.3 kJ mol^{-1} on Pd_6-SVG catalyst. However, a lower catalytic activity is exhibited for Pd_6-SVG comparing with that of Pd-SVG and Pd_4-SVG catalysts, as well as Pd (111) surface [3].

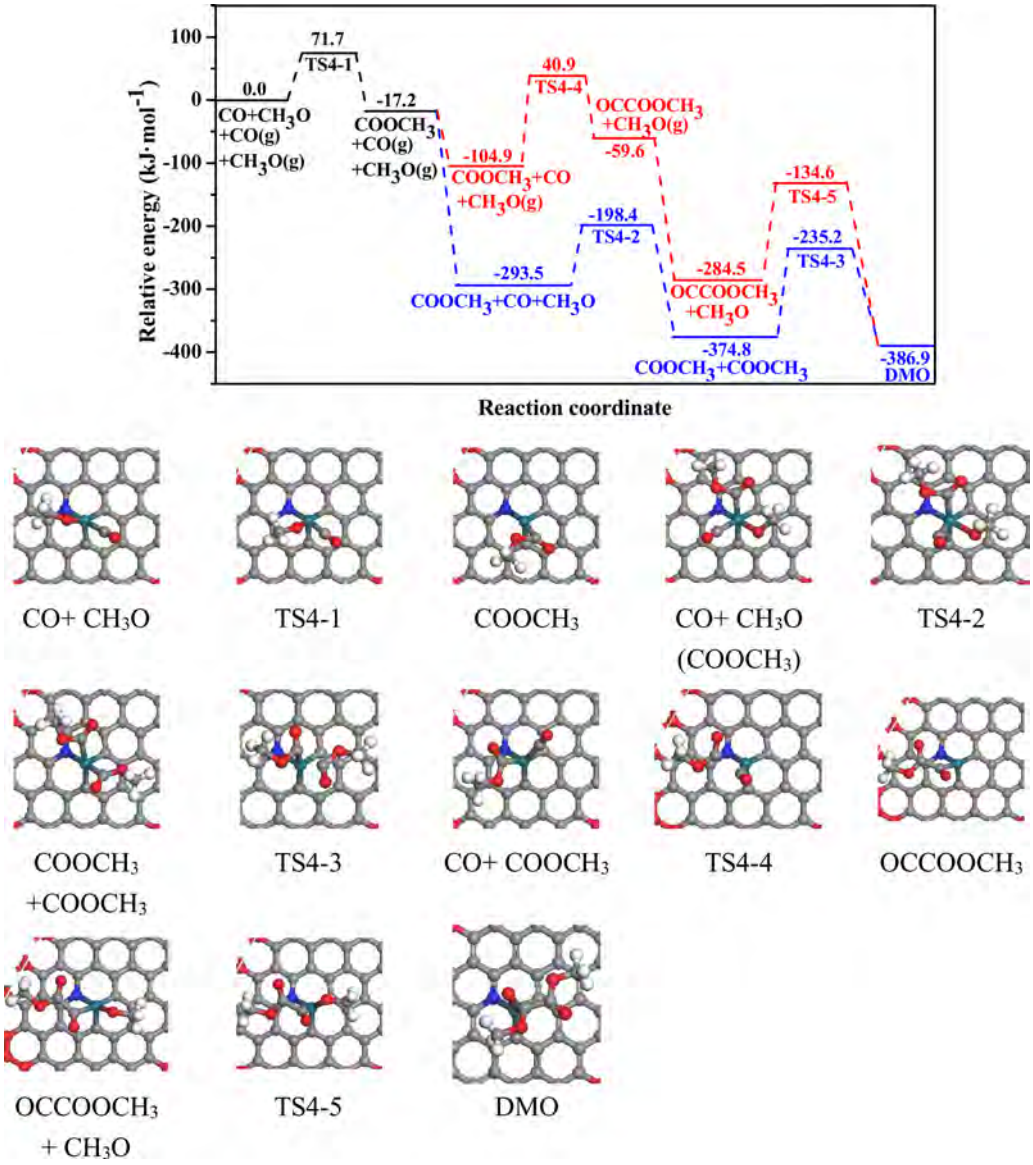

Fig. 7. Potential energy diagram of the correlation reaction of CO oxidative coupling to DMO and the configuration of initial states, transition states and final states on Pd-NVG.

3.2.4. The effect of size of Pd cluster on CO oxidative coupling to DMO

Both $COOCH_3$—$COOCH_3$ coupling and CO—$COOCH_3$ coupling pathways for the formation of DMO are obtained on Pd_n-SVG (n = 1, 4 and 6) catalysts. However, the most favorable pathway on Pd-SVG and Pd_4-SVG is $COOCH_3$—$COOCH_3$ coupling path, while CO—$COOCH_3$ coupling path is the advantageous path on Pd_6-SVG catalyst. In addition, energy barriers of rate-limiting steps in these three pathways are 114.1, 114.5 and 216.3 kJ mol^{-1} (see Fig. 6), respectively. It can be seen that activities of Pd_n-SVG (n = 1, 4 and 6) follow the order of Pd-SVG ≈ Pd_4-SVG > Pd_6-SVG. Obviously, Pd_6-SVG catalyst is with a lower activity for CO oxidative coupling to form DMO than Pd-SVG and Pd_4-SVG catalysts. Previous studies have shown the production of benzene by the cyclotrimerization of acetylene was observed on single-atom palladium at low temperature, because Pd atoms were activated by charge transfer from defect sites of MgO [95]. The similar result showed that a decrease of activity with an increase of the metal particle size, and single-atom catalysts were most active in the alcohol oxidation with Pd/meso-Al_2O_3 catalysts by Hackett et al. [96] Sun and co-workers [97] synthesized isolated Pt atoms anchored to graphene using the ALD technique, and Pt single-atom catalysts significantly improved catalytic activity in methanol electro oxidation reactions. In addition, a strong interaction between Pd metal and graphene is the key to prevent aggregation of single atoms on the surface [78]. In this case, different vacancies of graphene surface will play an essential role in stabilizing single-atom metal species and changing catalytic activity.

3.3. Effect of different defects of graphene on CO oxidative coupling reaction

3.3.1. The activity of Pd-NVG for the formation of DMO

Pd-SVG exhibits catalytically active and sufficiently stable, indicating that single-atom metal catalysts can offer a more effective way of utilizing noble metal elements. Thus, N-dopant were added to the single vacancy graphene in order to study the effect of heteroatoms on the chemical activity and selectivity. CO is adsorbed at single metal atom on the Pd-NVG surface with end-on mode, which is in agreement with that on Fe-N_4VG surface [91]. The same pathways with that on Pd-SVG are investigated, and the potential energy diagram is shown in Fig. 7. Intermediates $COOCH_3$ is firstly formed by CH_3O attacking the carbon atom of CO *via* TS4-1 on Pd-NVG surface with an energy barrier

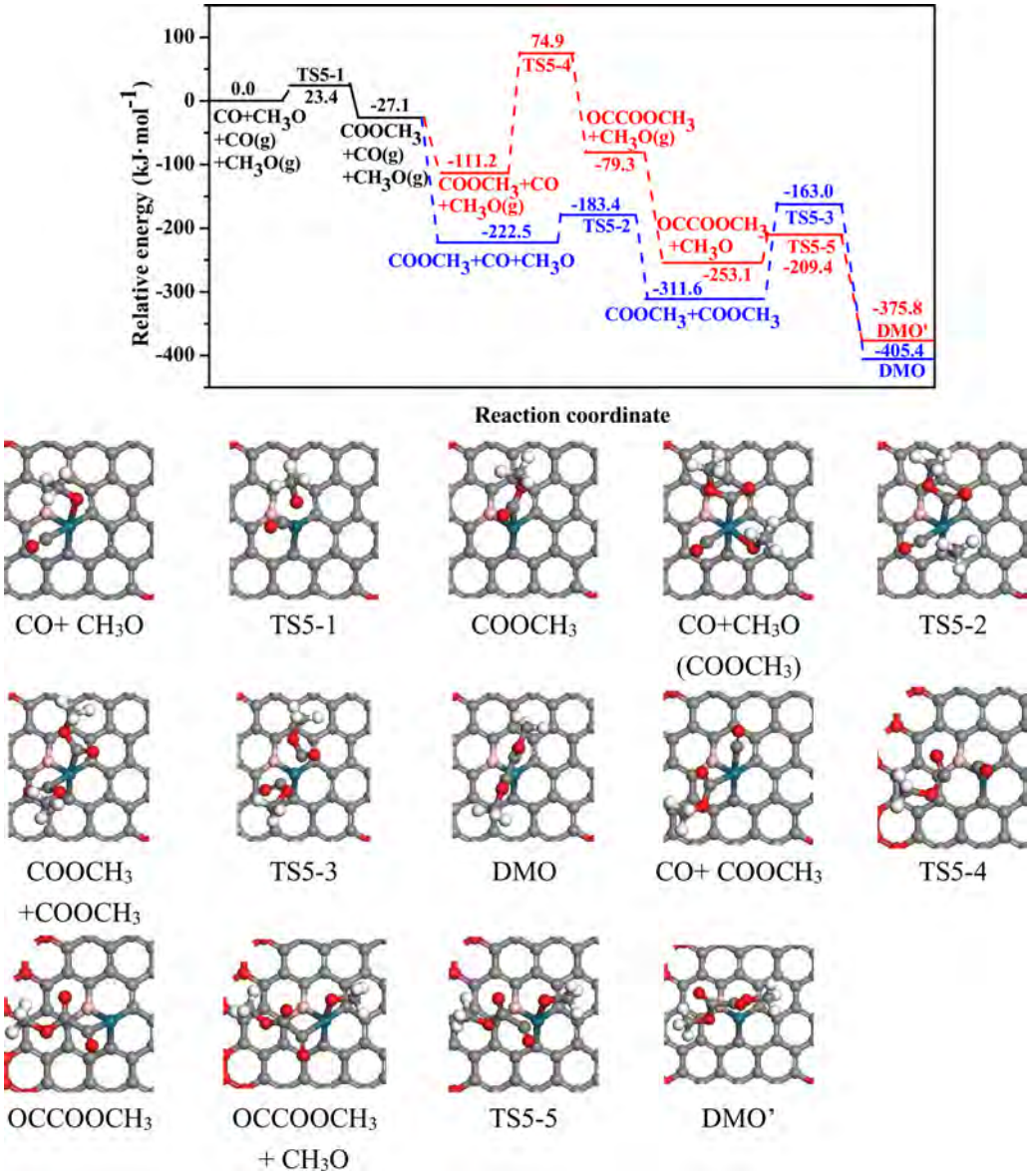

Fig. 8. Potential energy diagram of the correlation reaction of CO oxidative coupling to DMO and the configuration of initial states, transition states and final states on Pd-BVG.

of 71.7 kJ mol^{-1}. Staring from $COOCH_3$, two different elementary reactions can occur and two different intermediates can be obtained. The other $COOCH_3$ is formed *via* TS4-2 with a smaller energy barrier of 95.1 kJ mol^{-1}. And then two $COOCH_3$ coupling results in DMO *via* TS4-3, a higher energy barrier of 139.6 kJ mol^{-1} is needed to overcome. It can be seen that $COOCH_3$—$COOCH_3$ coupling is the rate-limiting step in Path 1. For CO—$COOCH_3$ coupling path in Path 2, $OCCOOCH_3$ resulting from the coupling of CO and $COOCH_3$ can connect with another CH_3O to form final product DMO, and this elementary reaction needs to overcome an energy barrier of 149.9 kJ mol^{-1}, which is the rate-limiting step. It implies that Path 1 is easier than Path 2 by comparing with the energy barrier. In addition, the catalytic activity of the Pd-NVG surface is lower than that of Pd-SVG.

3.3.2. CO oxidative coupling to DMO on Pd-BVG

B-doped graphene possesses long-time stability and excellent activity toward oxygen reduction reaction [98]. Thus, the effect of B-doped on the chemical activity is also considered. The $COOCH_3$—$COOCH_3$ coupling path (Path 1) is the most favorable pathway of CO oxidative coupling to DMO on Pd-BVG, and is shown in Fig. 8. For Path 1, $COOCH_3$—$COOCH_3$ self-coupling is the rate-limiting step, which needs to overcome high energy barrier of 148.6 kJ mol^{-1}. The formation of $COOCH_3$ and second $COOCH_3$ only need to overcome the low energy barriers of 23.4 and 39.1 kJ mol^{-1}. However, the CO—$COOCH_3$ coupling is the rate-limiting step with a higher energy barrier of 186.1 kJ mol^{-1} in Path 2. Therefore, CO oxidative coupling to DMO *via* $COOCH_3$—$COOCH_3$ self-coupling is the dominant pathway on Pd-BVG.

3.3.3. The formation of DMO on Pd_n-DVG

Besides, graphene with double carbon vacancy defect has been widely studied. In addition, Be-decorated graphene with double carbon vacancy defect are investigated for hydrogen storage applications, showing that the Be atom disperses well in the defective sites of graphene and prevents clustering [99]. Thus, the mechanism of CO oxidative coupling on the double-vacancy graphene supported Pd atom catalyst has also been systematically investigated. Initially, the active site on Pd-DVG has been confirmed at single Pd atom, and CO and CH_3O are adsorbed on this site. Previous studies have shown that single metal atom was also active site for the adsorption of CO and CHO on Pt-DVG [26]. The rate-determining step of $COOCH_3$—$COOCH_3$ coupling

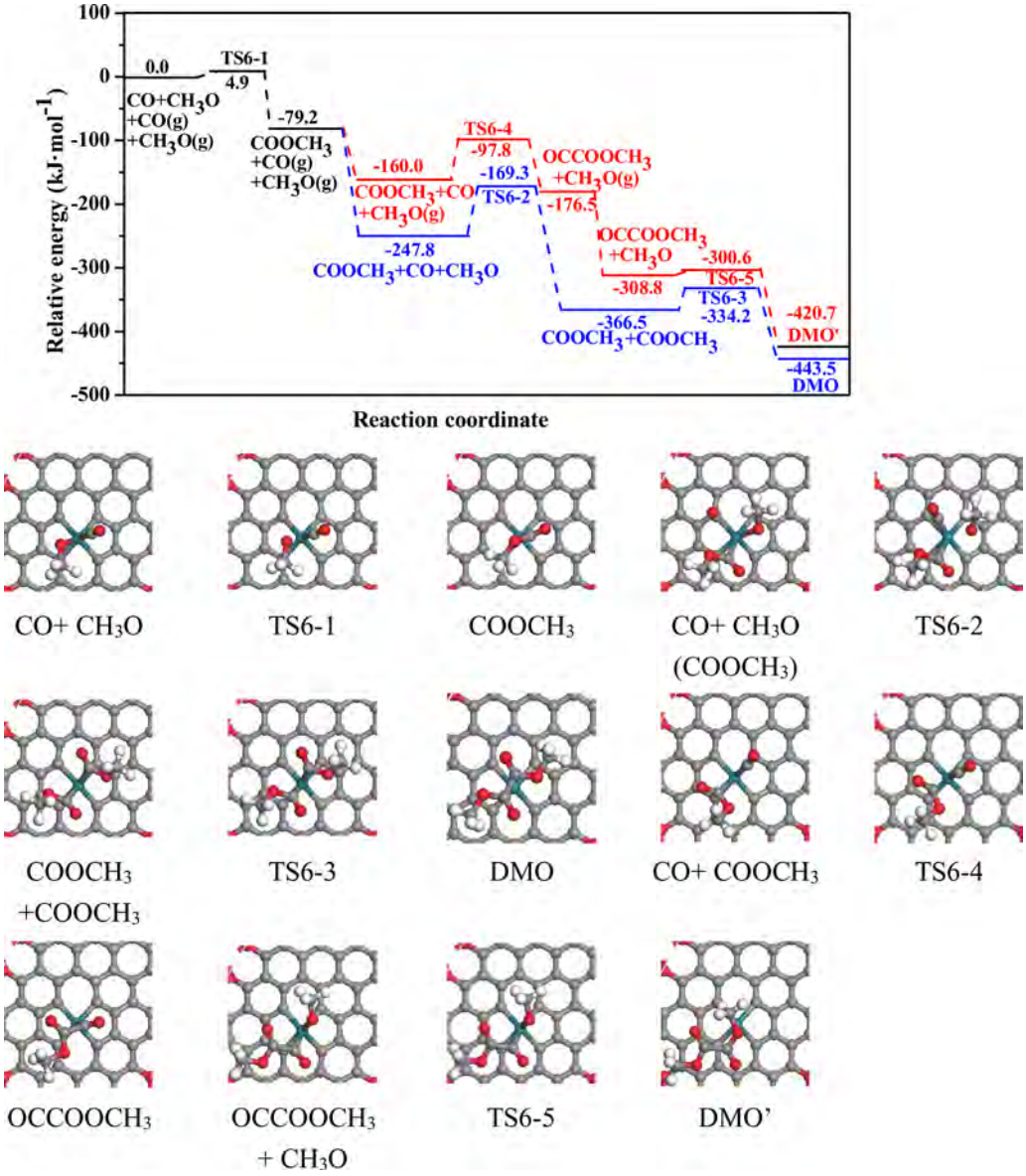

Fig. 9. Potential energy diagram of the correlation reaction of CO oxidative coupling to DMO and the configuration of initial states, transition states and final states on Pd-DVG.

path is the other $COOCH_3$ formation with an energy barrier of 78.5 kJ mol^{-1}, while the coupling step of CO and $COOCH_3$ is the rate-determining step in CO—$COOCH_3$ coupling route with an activation energy of 62.2 kJ mol^{-1}, as shown in Fig. 9. It indicates that Path 2 is the favorable pathway on the Pd-DVG catalyst, and Pd-DVG catalyst shows a high activity for CO oxidative coupling reaction.

We can also see that the reaction barrier greatly decreases on Pd-DVG (62.2 kJ mol^{-1}) catalyst comparing with that on Pd-SVG (114.1 kJ mol^{-1}), which implies that different vacancy concentrations on graphene surface will play an essential role in changing catalytic activity. Therefore, the rate-determining steps of the most favorable pathway for CO oxidative coupling to DMO on Pd_n (n = 4 and 6) clusters supported on double-vacancy graphene have also been studied, and the energy barriers on Pd-DVG, Pd_4-DVG and Pd_6-DVG are shown in Fig. 10. It can be seen that the energy barrier of rate-determining step on Pd_4-DVG (165.7 kJ mol^{-1}) is higher than that on Pd_4-SVG (114.5 kJ mol^{-1}), while it is on Pd_6-DVG (141.5 kJ mol^{-1}) lower than that on Pd_6-SVG (216.3 kJ mol^{-1}). It indicates that the size of Pd cluster has an unneglectable effect on the catalytic activity except for the vacancy concentrations. Obviously, single atom Pd supported on DVG catalyst still exhibits higher activity for CO oxidative coupling to DMO than Pd_4-DVG and Pd_6-DVG catalysts.

3.3.4. Comparing activities of Pd atom supported on different defective graphenes

It is obvious that different vacancy defects of graphene can affect the advantageous path and activity of CO oxidative coupling to DMO. Pd-DVG exhibits the most excellent catalytic activity for CO oxidative coupling reaction, CO—$COOCH_3$ coupling route is the favorable pathway and the energy barrier of rate-limiting step is just 62.2 kJ mol^{-1}. However, for the other three catalysts, the optimal formation pathway of DMO is $COOCH_3$—$COOCH_3$ coupling path, and forming new C—C bond is the rate-limiting step, the order of the energy barrier is Pd-SVG (114.1 kJ mol^{-1}) < Pd-NVG (139.6 kJ mol^{-1}) < Pd-BVG (148.6 kJ mol^{-1}) (Fig. 11). Obviously, Pd-SVG also shows relatively good catalytic activity compared to Pd-NVG and Pd-BVG. In the previous studies, Pd(111) surface is considered to be an excellent active surface, the rate-limiting step needs to overcome 114.6 kJ mol^{-1} for CO oxidative coupling to DMO [3]. Thus, Pd atom loading on double-vacancy and single-vacancy graphene show high catalytic activity for CO

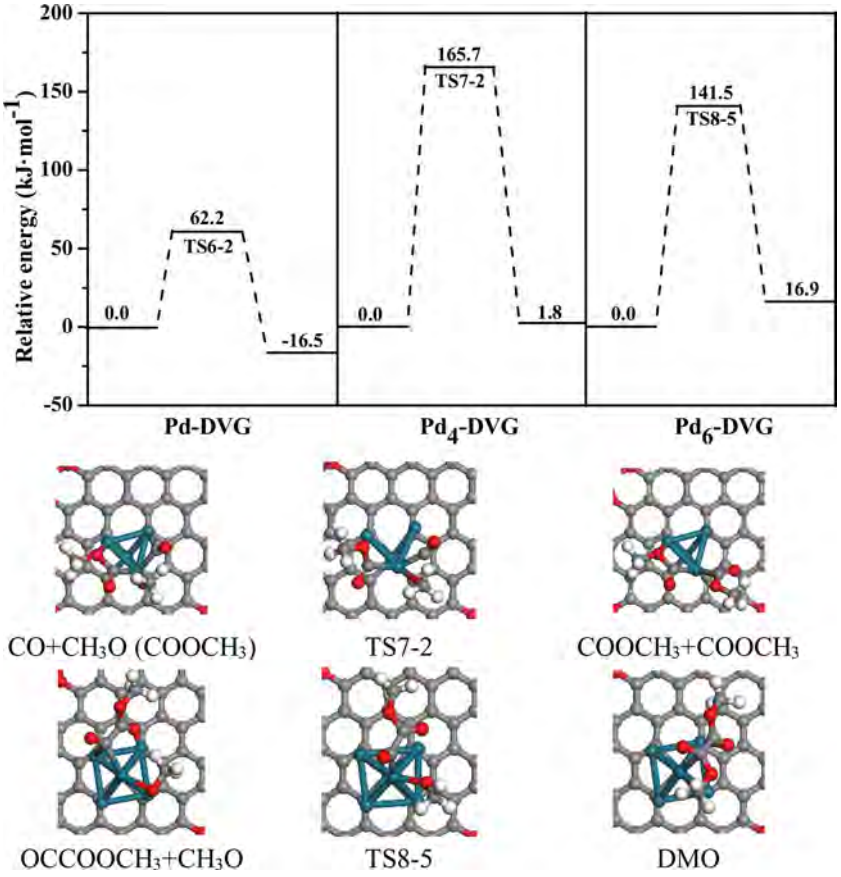

Fig. 10. The comparison of the simplified potential energy profile for the most favorable formation pathway of CO oxidative coupling to DMO on Pd-DVG, Pd_4-DVG and Pd_6-DVG.

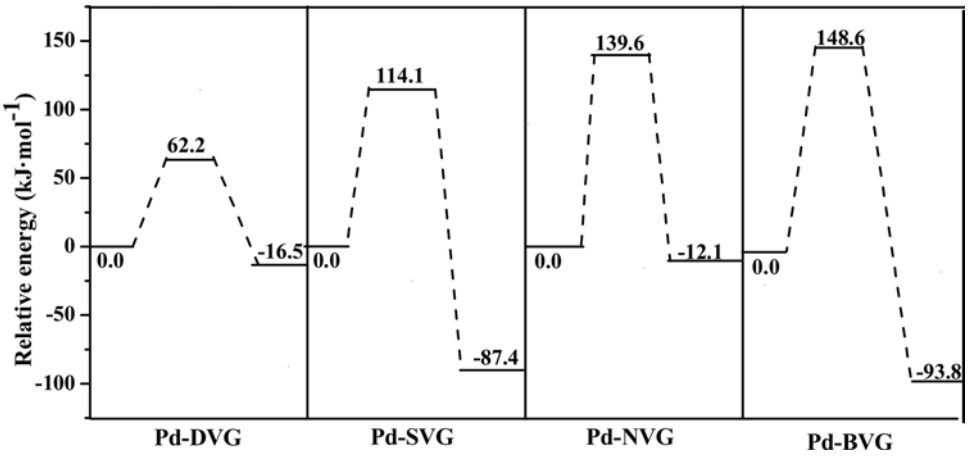

Fig. 11. The comparison of the simplified potential energy profile for the most favorable formation pathway of CO oxidative coupling to DMO on Pd-DVG, Pd-SVG, Pd-NVG and Pd-BVG.

oxidative coupling to DMO compared with the Pd(111) surface. Namely, Pd-DVG and Pd-SVG can not only maintain high activity but also maximize the utilization of metal atoms. However, the selectivity of DMO is an inevitable issue for CO oxidative coupling reaction, and previous experimental results showed that the exclusive formation of DMO over DMC on Pd-based catalyst [3,8]. In the next section, we focus on the issue of selectivity of DMO.

3.4. Selectivity of catalysts to DMO

DMC can be formed by CH_3O attacked $COOCH_3$, which lead to reduce the production of DMO. Thus, it is necessary to study the selectivity between DMO and DMC, and the difference between the formation barrier of DMC and that of DMO is used as the evaluation criteria. The above discussion shows that CO—$COOCH_3$ coupling path is the most favorable path to form DMO on Pd-DVG catalyst, while $COOCH_3$—$COOCH_3$ coupling path is the optimal path on Pd-SVG catalyst for CO oxidative coupling reaction. We considers the effect of CO on DMC generation because CO is excess in the actual reaction, starting with CO + CH_3O ($COOCH_3$), $COOCH_3$ is attacked by CH_3O to form DMC. As is revealed in Fig. 12, the formation barrier of DMC on the Pd-DVG catalyst is 125.8 kJ mol^{-1}. It is clear that the difference between

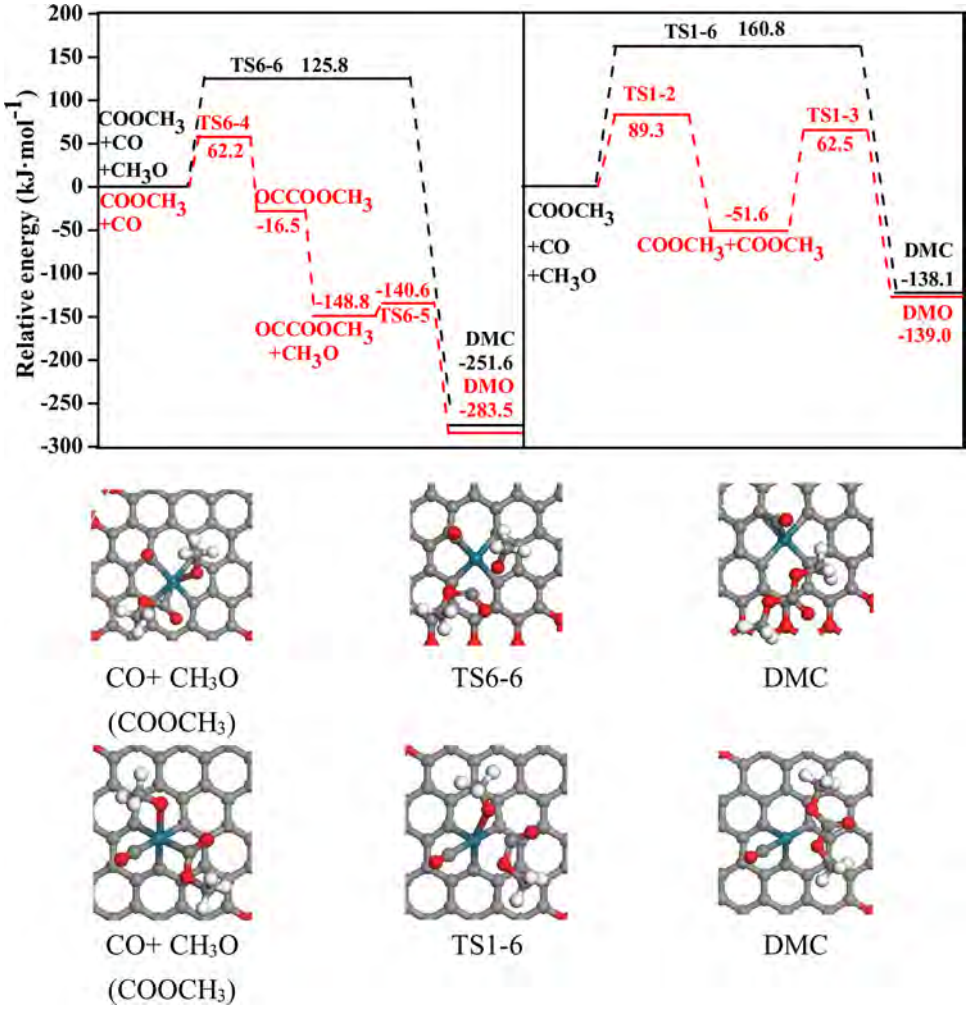

Fig. 12. The comparison of the simplified potential energy profile for the pathway of DMO and DMC formation together with structures of initial states, transition states and final states on Pd-DVG and Pd-SVG catalysts.

the formation barrier of DMO and that of DMC is 63.7 kJ mol^{-1}, namely, DMC is very difficult to appear on the Pd-DVG catalyst. In addition, we also considered the formation of DMC on the Pd-SVG catalyst which exhibits relatively high activity. A high energy barrier of 160.8 kJ mol^{-1} is necessary to form DMC, while the formation of DMO needs to overcome a smaller energy barrier of 114.1 kJ mol^{-1}. That is to say that DMO is also a major product rather than DMC on Pd-SVG catalyst. It can be seen that both Pd-DVG and Pd-SVG show high selectivity to DMO.

3.5. General discussion

In general, it can be seen that the preferred paths for CO oxidative coupling are various with the size of Pd cluster. The $COOCH_3$—$COOCH_3$ coupling path is followed on Pd-SVG and Pd_4-SVG, while the CO—$COOCH_3$ coupling path is the favorable path on Pd_6-SVG. In addition, the activity of the reaction is also affected by different cluster sizes, and the single-atom Pd supported on the single-vacancy graphene shows a very high catalytic activity. Further, the impact of different vacancy of graphene on reaction activity was considered in order to find a more efficient catalyst. The results show that the double-vacancy graphene supporting single-atom Pd exhibits amazing activity, in contrast, N-doped and B-doped catalysts show relative low activity comparing with the double-vacancy graphene catalyst. It is obvious that Pd-DVG and Pd-SVG can effectively reduce the cost of Pd-based catalyst and maintain the catalytic performance for CO oxidative coupling to DMO.

In addition, the catalytic selectivity between DMO and DMC on Pd-DVG and Pd-SVG catalyst was investigated. The result shows that DMO is easy to form on both Pd-DVG and Pd-SVG catalysts. In addition, Pd-DVG exhibits high activity for the formation of DMO due to low energy barrier. Therefore, Pd-DVG may be an optimistic catalyst for CO oxidative coupling to DMO. It is also believed that the insights derived from this study can provide a clue for the designing of high-efficient and low-cost catalyst.

4. Conclusions

In the premise of maintaining high activity, the study of reducing the amount of noble metal has been carried out in this work. A series of Pd_n (n = 1, 4 and 6) with different sizes anchored on single-vacancy graphene were firstly investigated by density functional theory (DFT) calculations. The results showed that the catalytic activity increased with the reduction of the Pd atomic number. Of more interest and importance, for CO oxidative coupling reaction, the Pd-SVG catalyst even exhibited similar high activity to Pd(111) surface which was considered as the highest activity surface in previous studies. The Pd-SVG catalyst makes it possible to develop supported Pd catalysts with low cost and high activity. On the other hand, the single Pd atom supported on different defective graphene were studied to reveal the effect of the vacancy type of graphene on reaction activity. It showed that the favorable pathway on Pd-DVG was $CO + CH_3O \rightarrow COOCH_3 + CO \rightarrow OCCOOCH_3 + CH_3O \rightarrow DMO$, while $COOCH_3$—$COOCH_3$ coupling path was the optimal pathway on Pd-SVG, Pd-

NVG and Pd-BVG. In particular, activities of CO oxidative coupling to DMO on Pd atom supported on different vacancy graphene catalysts followed the order of Pd-DVG > Pd-SVG > Pd(111) > Pd-NVG > Pd-BVG, suggesting that both Pd-DVG and Pd-SVG showed more excellent catalytic activity than that of Pd(111). Further, the selectivity of DMO was also an inevitable problem. The DFT result showed DMO was the main product on both Pd-DVG and Pd-SVG, and Pd-DVG exhibited more excellent activity. Therefore, Pd-DVG catalyst can be applied to effectively enhance the catalytic performance, maintain the selectivity, and greatly reduce cost.

Notes

The authors declare no competing financial interest.

Acknowledgments

We gratefully acknowledge financial support from the National Natural Science Foundation of China (Grant Nos. 21576178 and 21476155), the Key Projects of National Natural Science Foundation of China (No. 21736007), Research Project Supported by Shanxi Scholarship Council of China (No. 2016-030) and the Foundation of State Key Laboratory of Coal Conversion (No. J18-19-602).

References

[1] C.Z. Wang, L.P. Han, P.J. Chen, G.F. Zhao, Y. Liu, Y. Lu, High-performance, low Pd-loading microfibrous-structured Al-fiber@ns-AlOOH@Pd catalyst for CO coupling to dimethyl oxalate, J. Catal. 337 (2016) 145–156.
[2] S.Y. Peng, Z.N. Xu, Q.S. Chen, Z.Q. Wang, D.M. Lv, J. Sun, Y. Chen, G.C. Guo, Enhanced stability of Pd/ZnO catalyst for CO oxidative coupling to dimethyl oxalate: effect of Mg^{2+} doping, ACS Catal. 5 (2015) 4410–4417.
[3] Q.H. Li, Z.F. Zhou, R.P. Chen, B.Z. Sun, L.Y. Qiao, Y.G. Yao, K.C. Wu, Insights into the reaction mechanism of CO oxidative coupling to dimethyl oxalate over palladium: a combined DFT and IR study, Phys. Chem. Chem. Phys. 17 (2015) 9126–9134.
[4] L. Zhao, Y.J. Zhao, S.P. Wang, H.R. Yue, B. Wang, J. Lv, X.B. Ma, Hydrogenation of dimethyl oxalate using extruded Cu/SiO_2 catalysts: mechanical strength and catalytic performance, Ind. Eng. Chem. Res. 51 (2012) 13935–13943.
[5] X.X. Yu, J.G. Gao, Y.Z. Liu, System optimization model and path analysis for sustainable development of coal industry, Adv. Mater. Res. 986 (2014) 669–672.
[6] H.R. Yue, Y.J. Zhao, L. Zhao, J. Lv, S.P. Wang, J.L. Gong, X.B. Ma, Hydrogenation of dimethyl oxalate to ethylene glycol on a Cu/SiO_2/cordierite monolithic catalyst: enhanced internal mass transfer and stability, AIChE J. 58 (2012) 2798–2809.
[7] H. Yue, X.B. Ma, J.L. Gong, An alternative synthetic approach for efficient catalytic conversion of syngas to ethanol, Acc. Chem. Res. 47 (2014) 1483–1492.
[8] Z.N. Xu, J. Sun, C.S. Lin, X.M. Jiang, Q.S. Chen, S.Y. Peng, M.S. Wang, G.C. Guo, High-performance and long-lived Pd nanocatalyst directed by shape effect for CO oxidative coupling to dimethyl oxalate, Acs. Catal. 3 (2012) 118–122.
[9] Y. Ji, G. Liu, W. Li, W.D. Xiao, The mechanism of CO coupling reaction to form dimethyl oxalate over Pd/α-Al_2O_3, J. Mol. Catal. A: Chem. 314 (2009) 63–70.
[10] Q. Lin, Y. Ji, Z.D. Jiang, W.D. Xiao, Effects of precursors on preparation of Pd/(-Alumina catalyst for synthesis of dimethyl oxalate, Ind. Eng. Chem. Res. 46 (2007) 7950–7954.
[11] S.I. Uchiumi, K. Ataka, T. Matsuzaki, Oxidative reactions by a palladium–alkyl nitrite system, J. Organomet. Chem. 576 (1999) 279–289.
[12] T.J. Zhao, D. Chen, Y.C. Dai, W.K. Yuan, A. Holmen, Synthesis of dimethyl oxalate from CO and CH_3ONO on carbon nanofiber supported palladium catalysts, Ind. Eng. Chem. Res. 43 (2004) 4595–4601.
[13] S.Y. Peng, Z.N. Xu, Q.S. Chen, Y.M. Chen, J. Sun, Z.Q. Wang, M.S. Wang, G.C. Guo, An ultra-low Pd loading nanocatalyst with high activity and stability for CO oxidative coupling to dimethyl oxalate, Chem. Commun. 49 (2013) 5718–5720.
[14] Y. Lu, W. Chen, Sub-nanometre sized metal clusters: from synthetic challenges to the unique property discoveries, Chem. Soc. Rev. 41 (2012) 3594–3623.
[15] M. Marsault, G. Sitja, C.R. Henry, Regular arrays of Pd and PdAu clusters on ultrathin alumina films for reactivity studies, Phys. Chem. Chem. Phys. 16 (2014) 26458–26466.
[16] S. Tanabe, H. Matsumoto, Catalytic profiles of palladium clusters on zeolite in reduction of nitrogen monoxide with propane, J. Mater. Sci. Lett. 13 (1994) 1540–1542.
[17] M. Valden, J. Aaltonen, E. Kuusisto, M. Pessa, C.J. Barnes, Molecular beam studies of CO oxidation and CO-NO reactions on a supported Pd catalyst, Surf. Sci. 307 (1994) 193–198.
[18] H.A. Duarte, D.R. Salahub, NO adsorption on Pd clusters. A density functional study, Top. Catal. 9 (1999) 123–133.
[19] A.S. Wörz, K. Judai, S. Abbet, U. Heiz, Cluster size-dependent mechanisms of the CO + NO reaction on small Pd_n($n \leq 30$) clusters on oxide surfaces, J. Am. Chem. Soc. 125 (2003) 7964–7970.
[20] B. Kalita, R.C. Deka, Reaction intermediates of CO oxidation on gas phase Pd_4 clusters: a density functional study, J. Am. Chem. Soc. 131 (2009) 13252–13254.
[21] U. Heiz, A. Sanchez, S. Abbet, W.D. Schneider, Tuning the oxidation of carbon monoxide using nanoassembled model catalysts, Chem. Phys. 262 (2000) 189–200.
[22] S. Abbet, U. Heiz, H. Häkkinen, U. Landman, CO oxidation on a single Pd atom supported on magnesia, Phys. Rev. Lett. 86 (2001) 5950.
[23] W. Xiao, R. Zeng, L. Cheng, J.W. Wang, L.J. Jiang, L.G. Wang, Tunable catalytic reactivity of small palladium clusters supported on graphene: a first-principles study, RSC Adv. 5 (2015) 61861–61867.
[24] M. Kunaseth, T. Mudchimo, S. Namuangruk, N. Kungwan, V. Promarak, S. Jungsuttiwong, A DFT study of arsine adsorption on palladium doped graphene: effects of palladium cluster size, Appl. Surf. Sci. 367 (2016) 552–558.
[25] W. Sun, R.N. Shi, X.H. Wang, S.S. Liu, X.X. Han, C.F. Zhao, Z. Li, J. Ren, Density-functional theory study of dimethyl carbonate synthesis by methanol oxidative carbonylation on single-atom Cu_1/graphene catalyst, Appl. Surf. Sci. 425 (2017) 291–300.
[26] S. Back, J. Lim, N.Y. Kim, Y.H. Kim, Y. Jung, Single-atom catalysts for CO_2 electroreduction with significant activity and selectivity improvements, Chem. Sci. 8 (2017) 1090–1096.
[27] H. Yan, H. Cheng, H. Yi, Y. Lin, T. Yao, C.L. Wang, J.J. Li, S.Q. Wei, J.L. Lu, Single-atom Pd_1/graphene catalyst achieved by atomic layer deposition: remarkable performance in selective hydrogenation of 1 3-butadiene, J. Am. Chem. Soc. 137 (2015) 10484–10487.
[28] B.T. Qiao, A.Q. Wang, X.F. Yang, L.F. Allard, Z. Jiang, Y.T. Cui, J.Y. Liu, J. Li, T. Zhang, Single-atom catalysis of CO oxidation using Pt_1/FeO_x, Nat. Chem. 3 (2011) 634–641.
[29] S.F.J. Hackett, R.M. Brydson, M.H. Gass, I. Harvey, A.D. Newman, K. Wilson, A.F. Lee, High-activity, single-site mesoporous Pd/Al_2O_3 catalysts for selective aerobic oxidation of allylic alcohols, Angew. Chem. Int. Ed. 119 (2007) 8747–8750.
[30] X.F. Yang, A.Q. Wang, B.T. Qiao, J. Liu, T. Zhang, Single-atom catalysts: a new frontier in heterogeneous catalysis, Acc. Chem. Res. 46 (2013) 1740–1748.
[31] J.X. Liang, J. Lin, X.F. Yang, A.Q. Wang, B.T. Qiao, J.Y. Liu, T. Zhang, J. Li, Theoretical and experimental investigations on single-atom catalysis: Ir_1/FeO_x for CO oxidation, J. Phys. Chem. C 118 (2014) 21945–21951.
[32] J. Jones, H.F. Xiong, A.T. DeLaRiva, E.J. Peterson, H. Pham, S.R. Challa, G. Qi, S. Oh, M.H. Wiebenga, X.I.P. Hernández, Y. Wang, A.K. Datye, Thermally stable single-atom platinum-on-ceria catalysts via atom trapping, Science 353 (2016) 150–154.
[33] P.X. Liu, Y. Zhao, R.X. Qin, S.G. Mo, G.X. Chen, L. Gu, D.M. Chevrier, P. Zhang, Q. Guo, D.D. Zang, B.H. Wu, G. Fu, N.F. Zheng, Photochemical route for synthesizing atomically dispersed palladium catalysts, Science 352 (2016) 797–800.
[34] Q. Feng, S. Zhao, Y. Wang, J.C. Dong, W.X. Chen, D.S. He, D.S. Wang, J. Yang, Y.M. Zhu, H.L. Zhu, L. Gu, Z. Li, Y.X. Liu, R. Yu, J. Li, Y.D. Li, Isolated single-atom Pd sites in intermetallic nanostructures: high catalytic selectivity for semi- hydrogenation of alkynes, J. Am. Chem. Soc. 139 (2017) 7294–7301.
[35] H.J. Qiu, Y. Ito, W.T. Cong, Y.W. Tan, P. Liu, A. Hirata, T. Fujita, Z. Tang, M.W. Chen, Nanoporous graphene with single-atom nickel dopants: an efficient and stable catalyst for electrochemical hydrogen production, Angew. Chem. Int. Ed. 54 (2015) 14031–14035.
[36] S.J. Yu, X.X. Wang, Y.J. Ai, X.L. Tan, T. Hayat, W.P. Hu, X.K. Wang, Experimental and theoretical studies on competitive adsorption of aromatic compounds on reduced graphene oxides, J. Mater. Chem. A 4 (2016) 5654–5662.
[37] Y.B. Sun, S.B. Yang, Y. Chen, C.C. Ding, W.C. Cheng, X.K. Wang, Adsorption and desorption of U(VI) on functionalized graphene oxides: a combined experimental and theoretical study, Environ. Sci. Technol. 49 (2015) 4255–4262.
[38] S.B. Yang, L.J. Zhi, K. Tang, X.L. Feng, J. Maier, Efficient synthesis of heteroatom (N or S)-doped graphene based on ultrathin graphene oxide-porous silica sheets for oxygen reduction reactions, Adv. Funct. Mater. 22 (2012) 3634–3640.
[39] M.D. Bhatt, G. Lee, J.S. Lee, Oxygen reduction reaction mechanisms on Al-doped X-graphene (X = N, P, and S) catalysts in acidic medium: a comparative DFT study, J. Phys. Chem. C 120 (2016) 26435–26441.
[40] Z.Y. Wang, B. Yang, Y.L. Wang, Y.F. Zhao, X.M. Cao, P. Hu, Identifying the trend of reactivity for sp^2 materials: an electron delocalization model from first principles calculations, Phys. Chem. Chem. Phys. 15 (2013) 9498–9502.
[41] M.M. Ugeda, I. Brihuega, F. Guineam, J.M. Gómez-Rodrìguez, Missing atom as a source of carbon magnetism, Phys. Rev. Lett. 104 (2010) 096804.
[42] A.A. El-Barbary, R.H. Telling, C.P. Ewels, M.I. Heggie, P.R. Briddon, Structure and energetics of the vacancy in graphite, Phys. Rev. B 68 (2003) 144107.
[43] B.W. Jeong, J. Ihm, G.D. Lee, Stability of dislocation defect with two pentagon-heptagon pairs in graphene, Phys. Rev. B 78 (2008) 165403.
[44] G.D. Lee, C.Z. Wang, E. Yoon, N.M. Hwang, K.M. Ho, Vacancy defects and the formation of local haeckelite structures in graphene from tight-binding molecular dynamics, Phys. Rev. B 74 (2006) 245411.
[45] O.V. Yazyev, S.G. Louie, Topological defects in graphene: dislocations and grain boundaries, Phys. Rev. B 81 (2010) 195420.
[46] K.M. Fair, X.Y. Cui, L. Li, C.C. Shieh, R.K. Zheng, Z.W. Liu, B. Delley, M.J. Fold, S.P. Ringer, C. Stampfl, Hydrogen adsorption capacity of adatoms on double carbon vacancies of graphene: a trend study from first principles, Phys. Rev. B 87 (2013) 014102.
[47] Y.F. Zhu, T. Yi, B. Zheng, L.L. Cao, The interaction of C_{60} fullerene and carbon nanotube with Ar ion beam, Appl. Surf. Sci. 137 (1999) 83–90.
[48] A. Hashimoto, K. Suenaga, A. Gloter, K. Urita1, S. Iijima, Direct evidence for atomic defects in graphene layers, Nature 430 (2004) 870–873.
[49] M. Zhou, Y.H. Lu, Y.Q. Cai, C.C. Zhang, Y.P. Feng, Adsorption of gas molecules on transition metal embedded graphene: a search for high-performance graphene-based catalysts and gas sensors, Nanotechnology 22 (2011) 385–502.
[50] Y.Y. Liu, J. Wilcox, CO_2 adsorption on carbon models of organic constituents of gas

shale and coal, Environ. Sci. Technol. 45 (2010) 809–814.
[51] S.C. Xu, S. Irle, D.G. Musaev, M.C. Lin, Quantum chemical prediction of pathways and rate constants for reactions of CO and CO_2 with vacancy defects on graphite (0001) surfaces, J. Phys. Chem. C 113 (2009) 18772–18777.
[52] T.T. Jia, C.H. Lu, K.N. Ding, Y.F. Zhang, W.K. Chen, Oxidation of Pd_n (n = 1–5) clusters on single vacancy graphene: a first-principles study, Comput. Theor. Chem. 1020 (2013) 91–99.
[53] X.J. Qi, X. Guo, C.G. Zheng, Density functional study the interaction of oxygen molecule with defect sites of graphene, Appl. Surf. Sci. 259 (2012) 195–200.
[54] F.B.C. Machado, A.J.A. Aquino, H. Lischka, The electronic states of a double carbon vacancy defect in pyrene: a model study for graphene, Phys. Chem. Chem. Phys. 17 (2015) 12778–12785.
[55] J.Y. Dai, J.M. Yuan, P. Giannozzi, Gas adsorption on graphene doped with B N, Al, and S: a theoretical study, Appl. Phys. Lett. 95 (2009) 232105.
[56] O. Stephan, P.M. Ajayan, C. Colliex, P. Redlich, J.M. Lambert, P. Bernier, P. Lefin, Doping graphitic and carbon nanotube structures with boron and nitrogen, Science 266 (1994) 1683–1685.
[57] L.S. Panchakarla, K.S. Subrahmanyam, S.K. Saha, A. Govindaraj, H.R. Krishnamurthy, U.V. Waghmare, C.N.R. Rao, Synthesis structure, and properties of boron-and nitrogen-doped graphene, Adv. Mater. 21 (2009) 4726–4730.
[58] K.S. Subrahmanyam, L.S. Panchakarla, A. Govindaraj, C.N.R. Rao, Simple method of preparing graphene flakes by an arc-discharge method, J. Phys. Chem. C 113 (2009) 4257–4259.
[59] D. Golberg, Y. Bando, W. Han, K. Kurashima, T. Sato, Single-walled B-doped carbon, B/N-doped carbon and BN nanotubes synthesized from single-walled carbon nanotubes through a substitution reaction, Chem. Phys. Lett. 308 (1999) 337–342.
[60] L.R. Radovic, M. Karra, K. Skokova, P.A. Thrower, The role of substitutional boron in carbon oxidation, Carbon 36 (1998) 1841–1854.
[61] P. Ayala, R. Arenal, M. Rümmeli, A. Rubio, T. Pichier, The doping of carbon nanotubes with nitrogen and their potential applications, Carbon 48 (2010) 575–586.
[62] D.H. Deng, X.L. Pan, L. Yu, Y. Cui, Y.P. Jiang, J. Qi, W.X. Li, Q. Fu, X.C. Ma, Q.K. Xue, G.Q. Sun, X.H. Bao, Toward N-doped graphene via solvothermal synthesis, Chem. Mater. 23 (2011) 1188–1193.
[63] D.C. Wei, Y.Q. Liu, Y. Wang, H.L. Zhang, L.P. Huang, G. Yu, Synthesis of N-doped graphene by chemical vapor deposition and its electrical properties, Nano. Lett. 9 (2009) 1752–1758.
[64] B.R. Sathe, X.X. Zou, T. Asefa, Metal-free B-doped graphene with efficient electrocatalytic activity for hydrogen evolution reaction, Catal. Sci. Technol. 4 (2014) 2023–2030.
[65] B. Delley, From molecules to solids with the $DMol^3$ approach, J. Chem. Phys. 113 (2000) 7756–7764.
[66] J.P. Perdew, K. Burke, Y. Wang, Erratum: generalized gradient approximation for the exchange-correlation hole of a many-electron system, Phys. Rev. B 54 (1996) 16533.
[67] M. Xue, P. Cheng, N. Wang, Y.H. Li, S.P. Huang, Insight into the relationship between structural and electronic properties of bimetallic Rh_nPt_{55-n} (n = 0–55) clusters with cuboctahedral structure: DFT approaches, J. Clust. Sci. 27 (2016) 895–911.
[68] S. Grimme, Semiempirical GGA-type density functional constructed with a long-range dispersion correction, J. Comput. Chem. 27 (2006) 1787–1799.
[69] L. Wang, Q.Q. Luo, W.H. Zhang, J.L. Yang, Transition metal atom embedded graphene for capturing CO: a first-principles study, Int. J. Hydrogen Energy 39 (2014) 20190–20196.
[70] W.J. Hehre, L. Radom, P.R. Schleyer, J.A. Pople, Ab initio Molecular Theory, (1986) New York.
[71] A. Bergner, M. Dolg, W. Küchle, H. Stoll, H. Preu, Ab initio energy-adjusted pseudopotentials for elements of groups 13–17, Mol. Phys. 80 (1993) 1431–1441.
[72] X.Q. Liu, Y. Xue, Z.Y. Tian, J.J. Mo, N.X. Qiu, W. Chu, H.P. Xie, Adsorption of CH_4 on nitrogen- and boron- containing carbon models of coal predicted by density-functional theory, Appl. Surf. Sci. 285 (2013) 190–197.
[73] Y.H. Lu, M. Zhou, C. Zhang, Y.P. Feng, Metal-embedded graphene: a possible catalyst with high activity, J. Phys. Chem. C 113 (2009) 20156–20160.
[74] L.X. Ling, L.L. Fan, X. Feng, B.J. Wang, R.G. Zhang, Effects of the size and Cu modulation of Pd_n (n ≤ 38) clusters on Hg^0 adsorption, Chem. Eng. J. 308 (2017) 289–298.
[75] D.H. Lim, J. Wilcox, DFT-based study on oxygen adsorption on defective graphene-supported Pt nanoparticles, J. Phys. Chem. C 115 (2011) 22742–22747.
[76] N. Govind, M. Petersen, G. Fitzgerald, D. King-Smith, J. Andzelm, A generalized synchronous transit method for transition state location, Comp. Mater. Sci. 28 (2003) 250–258.
[77] T.A. Halgren, W.N. Lipscomb, The synchronous-transit method for determining reaction pathways and locating molecular transition states, Chem. Phys. Lett. 49 (1997) 225–232.
[78] G.M. Yang, X.F. Fan, S. Shi, H.H. Huang, W.T. Zheng, Stability of Pt_n cluster on free/defective graphene: a first-principles study, Appl. Surf. Sci. 392 (2017) 936–941.
[79] K.T. Chan, J.B. Neaton, M.L. Cohen, First-principles study of metal adatom adsorption on graphene, Phys. Rev. B 77 (2008) 235430.
[80] L.L. Fan, L.X. Ling, B.J. Wang, R.G. Zhang, The adsorption of mercury species and catalytic oxidation of Hg^0 on the metal-loaded activated carbon, Appl. Catal. A-Gen. 520 (2016) 13–23.
[81] Q.X. Zhou, C.Y. Wang, Z.B. Fu, L. Yuan, X. Yang, Y.J. Tang, H. Zhang, Hydrogen adsorption on palladium anchored defected graphene with B-doping: a theoretical study, Int. J. Hydrogen Energy 40 (2015) 2473–2483.
[82] J. Ren, W. Wang, D.L. Wang, Z.J. Zuo, J.Y. Lin, Z. Li, A theoretical investigation on the mechanism of dimethyl carbonate formation on Cu/AC catalyst, Appl. Catal. A-Gen. 472 (2014) 47–52.
[83] D. Sen, R. Thapa, K.K. Chattopadhyay, Small Pd cluster adsorbed double vacancy defect graphene sheet for hydrogen storage: a first-principles study, Int. J. Hydrogen Energy 38 (2013) 3041–3049.
[84] J. Liu, T.X. Liang, C. Wang, W.Z. Lai, Oxygen adsorption and CO desorption behavior of B-and N-doped vacancy defected nuclear graphite by DFT study, RSC Adv. 7 (2017) 3257–3264.
[85] M. Karabacak, S. Özçelik, Z.B. Güvenç, Structures and energetics of Pd_n (n = 2–20) clusters using an embedded-atom model potential, Surf. Sci. 507 (2002) 636–642.
[86] B. Kalita, R.C. Deka, Density functional studies on structure and reactivity of Pd_n clusters for n = 1–13, Bull. Catal. Soc. India 5 (2006) 110–120.
[87] R. Robles, S.N. Khanna, Oxidation of Pd_n (n = 1–7, 10) clusters supported on alumina/NiAl(110), Phys. Rev. B 82 (2010) 085428.
[88] J.G. Fang, B.W. Wang, Z.H. Li, G.H. Xu, Study on the reaction of CO coupling to oxalate, React. Kinet. Catal. Lett. 80 (2003) 293–301.
[89] F. Meng, G.H. Xu, Q.R. Guo, Kinetics of the catalytic coupling reaction of carbon monoxide to diethyl oxalate over Pd-Fe/α-Al_2O_3 catalyst, J. Mol. Catal. A: Chem. 201 (2003) 283–288.
[90] C.J. Cassady, B.S. Freiser, Gas-phase reactions of transition-metal ions with methyl nitrite and nitromethane, J. Am. Chem. Soc. 107 (1985) 1566–1573.
[91] C. Fan, M. Luo, W.D. Xiao, Reaction mechanism of methyl nitrite dissociation during co catalytic coupling to dimethyl oxalate: a density functional theory study, Chin. J. Chem. Eng. 24 (2016) 132–139.
[92] F. Meng, G.H. Xu, Q.R. Guo, H.F. Yan, M.Q. Chen, Kinetic study of carbon monoxide coupling reaction over supported palladium catalyst, Chem. Eng. Process. 43 (2004) 785–790.
[93] B.T. Qiao, J.X. Liang, A.Q. Wang, J.Y. Liu, T. Zhang, Single atom gold catalysts for low-temperature CO oxidation, Chin. J. Catal. 37 (2016) 1580–1586.
[94] Y.N. Tang, Z.X. Yang, X.Q. Dai, A theoretical simulation on the catalytic oxidation of CO on Pt/graphene, Phys. Chem. Chem. Phys. 14 (2012) 16566–16572.
[95] S. Abbet, A. Sanchez, U. Heiz, W.D. Schneider, A.M. Ferrari, G. Pacchioni, N. Rosch, Acetylene cyclotrimerization on supported size-selected Pd_n clusters (1 ≤ n ≤ 30): one atom is enough!, J. Am. Chem. Soc. 122 (2000) 3453–3457.
[96] S.F.J. Hackett, R.M. Brydson, M.H. Gass, I. Harvey, A.D. Newman, K. Wilson, A.F. Lee, High-activity, single-site mesoporous Pd/Al_2O_3 catalysts for selective aerobic oxidation of allylic alcohols, Angew. Chem. Int. Ed. 46 (2007) 8593–8596.
[97] S.H. Sun, G.X. Zhang, N. Gauquelin, N. Chen, J.G. Zhou, S.G. Yang, W.F. Chen, X.B. Meng, D.S. Geng, M.N. Banis, R.Y. Li, S.Y. Ye, S. Knights, G.A. Botton, T.K. Sham, X.L. Sun, Single-atom catalysis using Pt/graphene achieved through atomic layer deposition, Sci. Rep. 3 (2013) 1775.
[98] Z.H. Sheng, H.L. Gao, W.J. Bao, F.B. Wang, X.H. Xia, Synthesis of boron doped graphene for oxygen reduction reaction in fuel cells, J. Mater. Chem. 22 (2012) 390–395.
[99] M. Mahendran, B. Rekha, S. Seenithurai, R.K. Pandyan, S.V. Kumar, Hydrogen storage in beryllium decorated graphene with double vacancy and porphyrin defect – a first principles study, Funct. Mater. Lett. 10 (2017) 1750023.